한국해양공학회지 제19권 제5호, pp 16~25, 2005 (ISSN 1225-0767)

Evaluation of the Effect of Riser Support System on Global Spar Motion by Time-domain Nonlinear Hull/Mooring/Riser Coupled Analysis

BON-JUN KOO* AND MOO-HYUN KIM**

*Basic Design Part, Offshore Design Team, Samsung Heavy Industries Co. Ltd, Geoje, Korea

**Coastal and Ocean Engineering Program, Department of Civil Engineering, Texas A&M University, College Station USA.

KEY WORDS: Spar Platform, Pneumatic Cylinder, Buoyancy-can, Guide Frame, Multi-contact Coupling, Moon-pool, Hull-mooring-riser Coupling

ABSTRACT: *The effect of vertical riser support system on the dynamic behaviour of a classical spar platform is investigated. Spar platform generally uses buoyancy-can riser support system, but as water depth gets deeper the alternative riser support system is required due to safety and cost issues. The alternative riser support system is to hang risers off the spar platform using pneumatic cylinders rather than the buoyancy-can. The existing numerical model for hull/mooring/riser coupled dynamics analysis treats riser as an elastic rod truncated at the keel (truncated riser model), thus, in this model, the effect of riser support system can not be modeled correctly. Due to this reason, the truncated riser model tends to overestimate the spar pitch and heave motion. To evaluate more realistic global spar motion, mechanical coupling among risers, guide frames and support cylinders inside of spar moon-pool should be modeled. In the newly developed model, the risers are extended through the moon-pool by using nonlinear finite element methods with realistic boundary condition at multiple guide frames. In the simulation, the vertical tension from pneumatic cylinders is modeled by using ideal-gas equation and the vertical tension from buoyancy-cans is modeled as constant top tension. The different dynamic characteristics between buoyancy-can riser support system and pneumatic riser support system are extensively studied. The alternative riser support system tends to increase spar heave motion and needs damper system to reduce the spar heave motion.*

1. INTRODUCTION

Nowadays, offshore industry targets more oil and gas production in the 914 m (3000 ft) ~ 3048 m (10,000 ft) water depths. For this range of water depth, the classical spar and truss spar, semi-submersibles, and Floating Production Storage and Offloading (FPSO) are common production platform concepts for deep and remote wells. In particular, classical and truss spar are the most attractive concepts as deep and ultra deep water production platforms. Until recently, three classical and five truss spars are in production, four truss spars are in construction or installation, and a cell spar is under construction.

The design of risers and mooring lines has mostly been based on either uncoupled quasi-static analysis (model mooring and riser as massless linear springs, calculate hull responses, and estimate the mooring tension from static mooring load) or semi-coupled dynamic analysis (model mooring and riser as massless linear and nonlinear spring, calculated motions at the fairlead, and run line dynamics analysis for each mooring line). As water depth greatly increases, more inertia and damping effects can come from mooring lines and risers. Under this circumstance, uncoupled analysis methods may lead to inaccurate results. Thus, a reliable coupled dynamic analysis tool for the floating platform system is more and more important with increasing water depth. Time domain coupled analysis methods of floating platform and mooring lines have been reported by many researchers (Pauling and Webster, 1986; Kim et al., 1994, 1997, 2001; Ran et al., 1999; Ma et al., 2000; Gupta et al., 2000). In particular, Ran and Kim (1997) and Koo et al. (2004a, 2004b) developed a very efficient 3D hull/mooring/riser coupled dynamics program, WINPOST, based on combined matrix methods. In WINPOST, a global-coordinate-based finite element method (FEM), which was originally introduced by Garrett (1982), was employed for line dynamics. The floating platform is assumed to be a rigid body moving in the ocean environment as a result of wave, wind, and current forces. Linear translational/rotational springs and linear translational dampers are used at the connections between the platform and mooring lines and risers. The

제1저자 구본준 연락처: 경상남도 거제시 신현읍 장평리 530
055-630-8943 seanku@hanmail.net

classical spar platform, which is the target structure in this research, usually uses a vertical top-tensioned riser system with a dry tree on the deck. The vertical riser system is generally supported by freely floating buoyancy-can, but as the water depth gets deeper the required buoyant force increases due to increasing riser weight. It has been reported that the dimensions of a buoyancy-can are 4-meter in diameter and 80-meter long in 1324meters of water depth. Due to large volume of buoyancy-can, it makes installation difficult, particularly from safety point of view. Thus the alternative system is to hang the risers off the spar platform using pneumatic cylinders rather than the buoyancy-cans. The pneumatic cylinder allows the riser to move relative to one another and the spar hull. To evaluate pneumatic cylinder effects, the risers inside of the spar moon-pool should be fully modeled. In the existing numerical model, the risers are modeled up to keel and the effects from riser inside of spar moon-pool are approximated using a hull restoring coefficients (Tahar et al., 2002). The truncated model cannot accurately model the interaction between riser support system (buoyancy-can or pneumatic riser support system) and spar platform. The buoyancy-can effect inside of spar moon-pool developed by Koo (2003), and Koo et al. (2004b). Koo (2003) modeled the multiple-contact coupling between risers and riser guide frames using nonlinear gap spring model. The results show that restoring force and Coulomb damping force from riser buoyancy-can give more realistic spar pitch and heave motion (Koo et al., 2004b). The detailed derivation of the buoyancy-can effect is available in Koo (2003), and Koo et al. (2004b). In the present study, the riser inside of spar moon-pool are fully modeled, and thus pneumatic cylinder effects and additional contact forces and moments on the spar hull are considered.

The feasibility and dynamic effects of pneumatic cylinder riser support system are investigated for a 100 year hurricane condition of Gulf of Mexico. For simplification, the additional excitation on risers from moon-pool sloshing and riser-riser interactions are not considered in this study.

2. FORMULATION

2.1 Formulation of Hull/Mooring/Riser Coupling

In a time domain coupled dynamic analysis, the mooring, riser and platform dynamics are solved simultaneously as an integrated system. In the analysis, the hydrodynamic force on the platform are evaluated by 3 dimensional diffraction theory. The first-order wave forces, added mass and radiation damping, and the second-order mean and difference frequency forces on the platform are evaluated by WAMIT (Lee, 1995). The sum-frequency parts are not important for spar platform, thus not included in the motion analysis. The wave force linear and quadratic transfer functions (LTF and QTF) are calculated in the frequency domain, and then these forces are converted to the time domain using the two-term Volterra series expansion (Ran and Kim, 1997). The frequency dependent radiation damping is included in the form of a convolution integral in the time domain simulation.

For the static/dynamic analysis of the mooring and riser system, an extension of the theory developed for the dynamics of slender rods by Garrett (1982) is used in WINPOST. A brief summary of slender finite element formulation for a slender rod follows. Assuming no torque or applied external twisting moment, one can derive the linear momentum conservation equation with respect to a position vector $\vec{r}(s,t)$ that is a function of arc length *(s)* and time *(t)*:

$$-(B\vec{r}'')'' + (\lambda\vec{r}')' + \vec{q} = m\ddot{\vec{r}} \tag{1}$$

$$\lambda = T - B\chi^2 \tag{2}$$

$$T = T_0 + P_e A_e - P_i A_i \tag{3}$$

where, prime and dot denotes spatial and time derivative, respectively, B is bending stiffness, T, the local effective tension, χ, the local curvature, m, the mass per unit length, $\vec{q}$, the distributed force on the rod per unit length, T_0, the local tension, P_e, the external pressures, P_i, the internal pressures, A_e and A_i are external and internal cross-sectional areas. The scalar variable λ can be regarded as a Largrange multiplier. If the rod is assumed to be in extensible, the following condition must be satisfied:

$$\vec{r}' \cdot \vec{r}' - 1 = 0 \tag{4}$$

If the rod is extensible, the following relation can be used

$$\frac{1}{2}(\vec{r}' \cdot \vec{r}' - 1) = \frac{T}{EA_t} \approx \frac{\lambda}{EA_t} \tag{5}$$

$$A_t = A_e - A_i \tag{6}$$

For these equations, the geometric nonlinearity is fully considered there is no special assumption made concerning the shape or orientation of the mooring lines, as long as the rod remains elastic. The normal component of the distributed external force on the rod per unit length, q_n, is given by the generalized Morison equation (e.g. Paulling and Webster, 1986).

$$q_n = C_I \rho A_e \dot{v}_n + \frac{1}{2} C_D \rho D |v_{nr}| v_{nr} + C_m \rho A_e \ddot{r}_n \quad (7)$$

where C_I, C_D, and C_m are inertia, drag and added mass coefficients, and $\dot{v}_n$, v_{nr}, and $\ddot{r}_n$ are normal fluid acceleration, normal relative velocity, and normal structure acceleration, respectively. The symbols ρ and D are fluid density and local diameter. in addition, the effective weight, or net buoyancy, of the rod should be included in q_n, as a static load. To develop the finite element formulation, consider a single element of length L, and use the following expression:

$$\vec{r}(s, t) = \sum_i A_i(s) \vec{U}_i(t) \quad (8)$$

$$\lambda(s, t) = \sum_m P_m(s) \lambda_m(t) \quad (9)$$

where A_i and P_m are Hermitian cubic and quadratic interpolation functions defined on the interval $o \le s \le L$. Using equation (8) and (9), equation (1) can be reduced to the following equation by the Galerkins method and integration by parts (Garrett, 1982):

$$\int_0^L [B\vec{r}''A_i'' + \lambda\vec{r}'A_i' - \vec{q}A_i' + m\ddot{\vec{r}}A_i] ds$$
$$= B\vec{r}'A_i' \Big|_0^L + \lambda\vec{r}' - (B\vec{r}'')'A_i \Big|_0^L \quad (10)$$

where it is assumed that the shape function A_i continuous on the element. The first boundary term of the right-hand side is related to the moments on the ends, and the second term is the force on the ends, i.e. they are natural boundary conditions. If equation (4) is used, we obtain:

$$\int_0^L P_m \left\{ \frac{1}{2} (\vec{r}'\vec{r}' - 1) - \frac{\lambda}{EA_i} \right\} ds = 0 \quad (11)$$

The position vector, its tangent, and the Lagrange multiplier are selected to be continuous at a node between adjacent element.

Elements are combined using the continuity of $\vec{r}$, $\vec{r}'$, and λ. The natural boundary conditions at joint cancel out, leaving those conditions applicable at the ends of the rod. The upper ends of these risers and mooring lines are connected to the hull through a generalized translational and rotational spring that can also model both fixed and hinged boundary conditions at its limit. The forces and moments proportional to the relative displacements are transmitted to the hull at the connection points. The transmitted force from mooring lines and risers to the platform are given by:

$$F_p = K(Tu_p - u_I) + C(T\dot{u}_p - \dot{u}_I) \quad (12)$$

where K is the stiffness matrix, C, the damping matrix, T, the transformation matrix between the platform origin and connection point, u_p and u_I are displacement vectors of the platform and connection point.

The hull response equation is combined into the mooring line equation in the time-domain as follows:

$$(M + M_a(\infty))\ddot{u}_p + \int_0^\infty R(t-\tau)\dot{u}_p d\tau + K_H u_p$$
$$= F_{(D)} + F^{(1)} + F^{(2)} + F_p + F_{WD} \quad (13)$$

where, M and M_a are structure mass and added mass, R the retardation function (inverse cosine Fourier transform of radiation damping), K_H the hydrostatic restoring coefficients, F_D the drag force matrix on the hull, $F^{(1)}$, $F^{(2)}$ the first- and second-order wave load matrices on the hull, F_p the transmitted force matrix from the interface, and F_{WD} the wave drift damping force matrix. The added mass at infinite frequency is obtained from Kramers-Kroing relation. For the time series of $F^{(1)}$, $F^{(2)}$, and F_{WD} a two-term Volttera series is used. From above time-domain equation of motion, the hull/mooring line/riser coupled analysis can be achieved.

2.2 Formulation of Buoyancy-can Riser Support System

In this section, the hull and riser coupling effects inside of spar moon-pool are formulated. As mentioned in introduction, the spar platform generally uses vertical production risers which are supported by buoyancy-can or, pneumatic cylinders. There are several guide frames inside of the spar moon-pool, and the function of these guide frames is to restrict the riser horizontal motion and prevent collision. Thus, when the spar heels, the buoyancy-cans give additional restoring moments through contact forces to resist the hull pitch/roll motions. In addition, the contact forces at support guide frames induce Coulomb friction to resist the hull heave motion.

The shape of buoyancy-can is circular cylinder, and the guide frame is also a circular plate with a pening. Thus, the contact between buoyancy-can and riser support frame can be modeled as point contact. In the numerical modeling, the contact horizontal force is modeled as the concentration force caused by very stiff translational spring. Thus, the resulting contact forces affect both the motion of the riser and spar hull. Since a spar has everal guide frames, the riser and the hull have multi-contact couplings. In equation (10), the first term on the right-hand side is the bending moment and second term in the right-hand side is the force at the node. if there is no multi-contact coupling, these two terms cancel to satisfy the compatibility between elements, However, when the support guide frame touches the riser, the contact force is applied to the node and the second term of equation (10) from which the contact force can be calculated does not vanish. Fig. 1 shows the schematic drawing of spar hull and buoyancy-can riser support system.

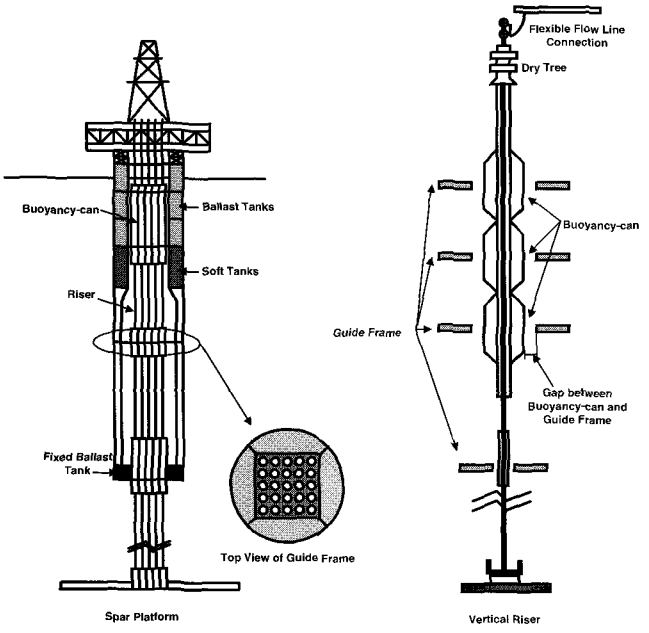

Fig. 1 Spar hull, buoyancy-can and guide-frame

The detail derivation of the multi-contact coupling between risers and riser guide frames is available in Koo et al. (2004). The brief description of multi-contact coupling between risers and riser guide frames is as follows:

Linear spring approximation model

$$F_R = K(Tu_p - u_r) \tag{14}$$

Piecewise-linear gap-contact spring model

$$F_R = K(Tu_p - u_r - \triangle_i) \text{ when, } (Tu_p - u_r) \geq \triangle_i \tag{15}$$

$$F_R = 0 \text{ when, } -\triangle_i < (Tu_p - u_r) < \triangle_i \tag{16}$$

$$F_R = K(Tu_p - u_r - \triangle_i) \text{ when, } -\triangle_i \leq (Tu_p - u_r) \tag{17}$$

Piecewise-quadratic gap-contact spring model

$$F_R = K(Tu_p - u_r - \triangle_i)^2 \text{ when, } (Tu_p - u_r) \geq \triangle_i \tag{18}$$

$$F_R = 0 \text{ when, } -\triangle_i < (Tu_p - u_r) < \triangle_i \tag{19}$$

$$F_R = -K(Tu_p - u_r - \triangle_i)^2 \text{when, } -\triangle_i \leq (Tu_p - u_r) \tag{20}$$

Cubic Spring Approximation

$$F_R = K(Tu_p - u_r)^3 \tag{21}$$

where, u_p is displacement vector of the guide frame, u_r the displacement vector of the contact point of the riser, F_R the horizontal contact force matrix. Fig. 2 shows force displacement relation of each contact spring model.

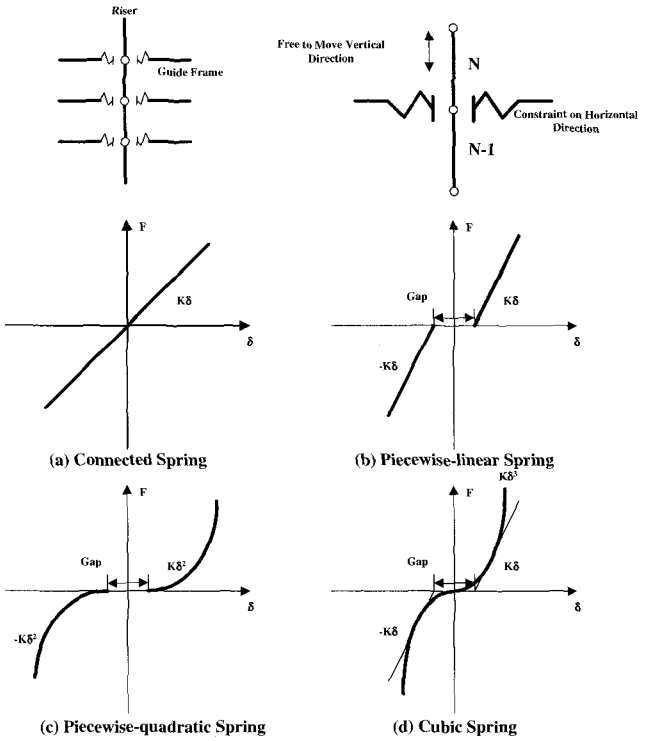

Fig. 2 Schematic drawing of force displacement relation of each contact spring model

The Coulomb damping between riser guide frames and risers inside of the spar platform modeled by

$$F_C = \mu sgn(Tu_{f3} - u_{r3})\sqrt{F_{R1}^2 + F_{R2}^2} \quad (22)$$

where, u_{p3} and u_{r3} are the vertical displacement vector of the riser guide frames and riser, μ is the frictional coefficient between riser and riser guide frames, and F_{R1} and F_{R2} are the horizontal contact force between riser and riser guide frame.
The contact force and moment on the platform can be obtained by following formula

$$F_{pl} = -(F_R + F_C) \quad (23)$$
$$M = (P\times - F_R) + (P\times - F_C) \quad (24)$$

where, F_{pl} and M are force and moment matrix on spar platform, and P represents position vector (in body coordinate) of the platform where the coupling occurs.

2.3 Formulation of Pneumatic Cylinder Riser Support System

The pneumatic cylinder riser support system can be modeled as ideal-gas equation. The pneumatic cylinder for each riser act as a soft spring and gives additional restoring force to the platform motion. Fig. 3, and 4 show pneumatic riser support system.

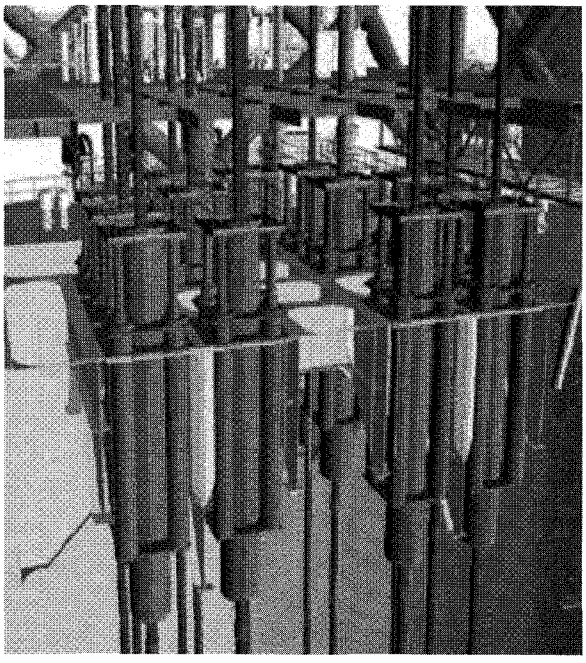

Fig. 3 Pneumatic cylinder riser support system (Courtesy, Aker Maritime)

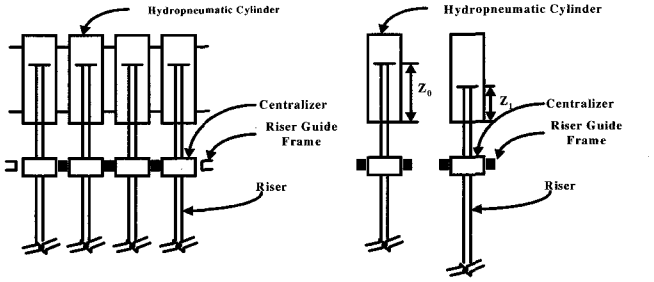

Fig. 4 Schematic drawing of pneumatic riser support system

The pneumatic cylinder force on the riser and platform can be modeled as follows:

$$P_0 V_0 = P_1 V_1 \quad (25)$$
$$P_1 A Z_1 = P_0 A Z_0 \quad (26)$$
$$F_1 Z_1 = F_0 Z_0 \quad (27)$$
$$F_1 = F_0 Z_0 / Z_1 \quad (28)$$

where, P_0 and P_1 are the pressure, V_0 and V_1 are the volume inside, A is the cross sectional area of the cylinder, Z_0 and Z_1 are the stroke, F_0 and F_1 are the tension.
In the equation (27), Z_1 can be expressed as follows:

$$Z_1 = Z_0 - (Tu_{pn3} - u_{r3}) \quad (29)$$

where, u_{pn3} and u_{r3} are the vertical displacement vector of the pneumatic cylinder and riser.
The dynamic top tension from pneumatic cylinder can be modeled as:

$$F_{pn} = T_0\{Z_0/(Z_0 - Tu_{pn3} - u_{r3})\} \quad (30)$$

where, F_{pn} is pneumatic cylinder force on the riser and T_0 represent initial tension. The force and moment on the platform are identical to equation (23) and (24)

3. SPECIFICATION OF SPAR PLATFORM

The specifications of the spar platform used in the present study are summarized in Table 1. The spar platform has 14 chain-wire-chain mooring lines and 23 steel vertical risers. The arrangement of mooring lines and risers are shown in Fig. 5 The mooring line characteristics are shown in Table 2. The spar platform

has 18 production risers, 1 drilling riser, 2 water injection risers, 1 oil export and 1 gas export riser. Table 3 shows riser characteristics.

Table 1 Spar hull characteristics

Classical spar (3000ft)	
Total Displacement (Ton)	2.205E+8
Draft (m)	198.12
Hard tank depth (m)	67.06
Well bay dimension (m^2)	17.7X17.7
KB (m)	164.6
KG (m)	96.71
Radius of gyration (m)	67.36 pitch, 8.96 yaw
Drag force coefficient	1.0
Center of pressure for wind area (m)	22 above MWL
Design Depth (m)	914.4

Table 2 Spar mooring system characteristics

Mooring lines	Dry/Wet weight	Axial Stiffness	Added Mass
	N/m	kN/m	kg/m
K4 Studless chain 133.4 mm	3.71E+2/3.23E+2	1.33E+6	4.82E+1
Sheathed wire 136.5 mm	9.91E+1/1.98E+1	1.63e+6	1.98E+1

Table 3 Riser system characteristics

Riser	No.	Top tension	Axial Stiffness	Dry/Wet weight
		kN	kN/m	N/m
Drilling	1	4.167E+3	1.201E+7	5.95E+2/3.66E+2
Production	18	2.344E+3	2.994E+6	3.01E+2/1.95E+2
Water injection	2	1.443E+3	1.837E+6	1.03E+2/6.46E+2
Oil export	1	1.872E+3	4.626E+6	2.96E+2/1.63E+2
Gas export	1	9.53E+2	4.626E+6	2.08E+2/7.45E+2

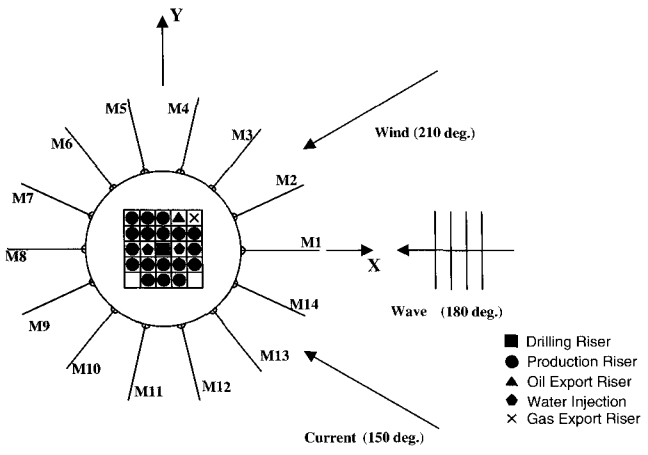

Fig. 5 Mooring lines/risers configuration and environmental direction

4. DESCRIPTION OF CASE STUDY AND DESIGN ENVIRONMENTAL CONDITION

The simulation is conducted for two different spar platforms with free decay simulations and the 100-year hurricane condition for the Gulf of Mexico. In the numerical modeling, the current is assumed to be steady and the irregular wave unidirectional. The wave heading is 180 degree with respect to the global axis. A JONSWAP spectrum of significant wave height 12.19m, peak period 14sec, and overshoot parameter 2.5 was selected to present a typical 100-year hurricane in the Gulf of Mexico. The hurricane induced current flows from 30 degrees right of wave direction. The current velocity is assumed to be 1.07 m/sec from mean water level to 60.96 m water depths and is reduced to 0.091 m/sec at 91.44 m and zero at 914.4 m. The wind speed used is 41.1 m/sec (i.e. 1-hour averaged) at 10 m above mean water level and wind direction is 30 degrees left of wave direction. API (America Petroleum Institute) wind spectrum is used for the generation of time varying wind forces (API RP-2A WSD, 1994).

The riser support system used in the simulations are summarized in Table 4. The Case A Spar platform uses pneumatic cylinders for supporting riser. Thus, the risers are hanging off the topside of spar platform. In the Case A modeling, all the pneumatic cylinders are modeled as nonlinear spring rather than constant top tension (i.e. buoyancy-can) on top of the risers, and guide frames are modeled as cubic spring with a large spring constant. Due to absence of the buoyancy-can, rubber type centralizers protect the risers when it touches the guide frames. The rubber type centralizer is modeled as a cubic spring. The Case B Spar platform uses buoyancy-cans for the supporting risers, and the risers are modeled as a freely standing structure. In the Case B modeling, all the buoyancy-cans are modeled as constant top tension on top of the risers and uses the identical guide frame model (i.e. cubic spring) as Case A. For simplification, the Coulomb damping effect between riser and riser guide frames is not considered

To evaluate damping ratio and natural period of the spar platform, free decay simulations are conducted. After free decay simulations, the 100-year hurricane simulations are conducted for both spar platforms.

Table 4 Summary of the riser modeling

	Riser	Guide Frame	Riser Support Type
CASE A	Fully Modeled	Cubic Spring	Pneumatic Cylinder
CASE B	Fully Modeled	Cubic Spring	Buoyancy-can

5.RESULTS AND DISCUSSION

5.1 Free Decay Simulation Results

Free decay simulation results are shown in Fig. 6 through Fig. 13. The results show that pneumatic cylinders do not change the surge and pitch motion significantly, but it is interesting to notice that heave motion is totally different due to additional heave restoring force from pneumatic cylinders. To see the pneumatic cylinder effect, in the heave free decay simulation, Coulomb damping effect is not considered. The Case A heave free decay time series shows that the first down crossing peak is larger than Case B. The reason is that large initial heave offset stiffens the pneumatic cylinders, and it makes springing-like phenomena in first down crossing peak. After first down crossing heave motion, the Case A Spar has smaller motion amplitudes and period than those of the Case B Spar platform. The heave natural period difference is clearly shown in the Fig. 8 and 9. Fig. 10 and 11 show the time series of the top tension on the production riser in heave free decay simulation. Fig. 10 shows the dynamic top tension from pneumatic cylinder. Dynamic top tension time series show identical phase as heave motion. These results clearly show that the dynamic forces on the spar platform have 180-degree phase difference and give additional heave restoring force on the spar platform. Fig. 10 shows that the constant buoyant force from buoyancy-can. The free decay simulation results are summarized in Table 5. The surge, pitch, and heave damping ratios are calculated by averaging first seven peaks from free decay simulations.

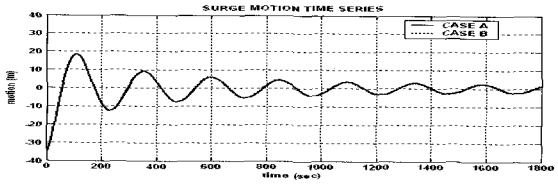

Fig. 6 Surge free decay time series

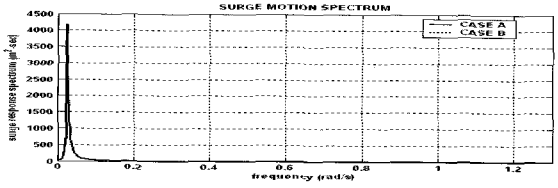

Fig. 7 Surge free decay spectrum

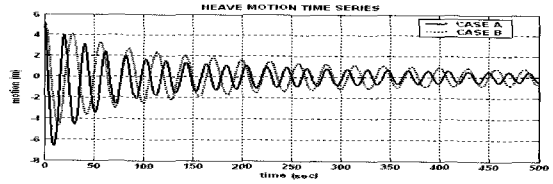

Fig. 8 Heave free decay time series

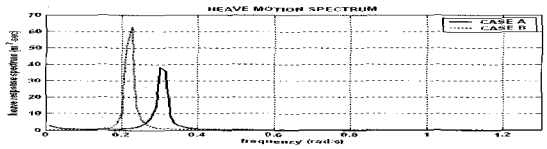

Fig. 9 Heave free decay Spectrum

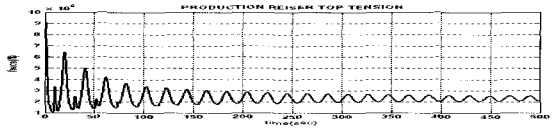

Fig. 10 Production riser topside time Series (CASE A)

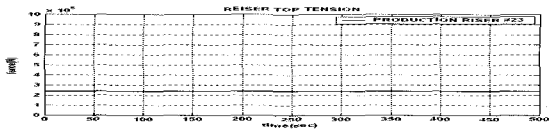

Fig. 11 Production riser topside time Series (CASE B)

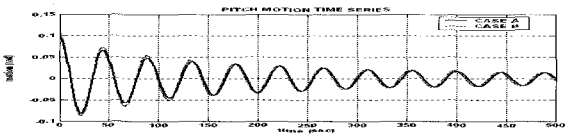

Fig. 12 Pitch free decay time series

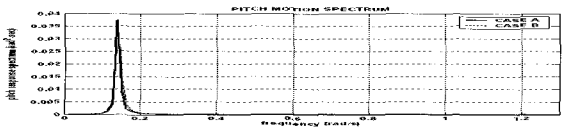

Fig. 13 Pitch free decay spectrum

Table 5 Summary of free decay simulation

	Surge		Heave		Pitch	
	CASE A	CASE B	CASE A	CASE B	CASE A	CASE B
T_N (sec)	257.2	257.2	20.9	27.8	45.5	45.5
ζ (%)	6.0	5.9	3.1	2.7	3.5	3.5

5.2 100-year Hurricane Simulation Results

Fig. 14, 15 and 16 show the wave time series, wave spectrum, and wind velocity spectrum which are used in simulations.

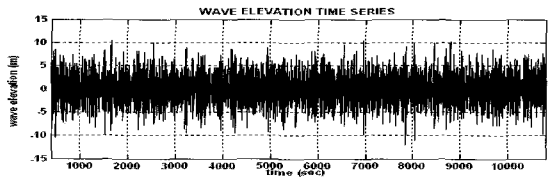

Fig. 14 100-year hurricane wave time series

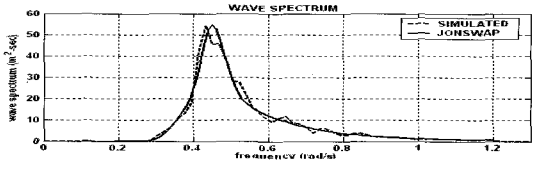

Fig. 15 100-year hurricane wave spectrum

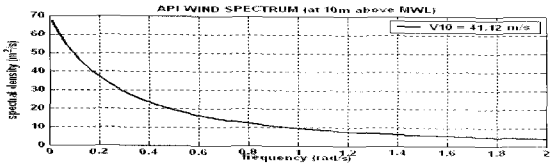

Fig. 16 100-year hurricane wind velocity spectrum

The 100-year hurricane simulation results are shown in Fig. 17 through 29. The results show that the Case A Spar and Case B Spar have almost identical surge and pitch responses. This means that the contribution from pneumatic cylinders is not significant in surge and pitch motions. However, the heave response of Case A Spar is much larger than that of Case B Spar. Table 6 and 7 show that the Case A Spar and the Case B Spar have almost identical low frequency heave motion, but Case A Spar has 3.5 times larger wave frequency motion than Case B Spar platform. The larger wave frequency motion is caused by the additional heave restoring force from pneumatic cylinders that increases the heave natural frequency and therefore increases the heave wave frequency motion significantly. Due to the large wave frequency heave motion, the riser top tensions also show large standard deviation in Case A Spar platform. The summary of statistics, time series, and spectrum of riser top tension are shown in Table 8 and Fig. 26 through 28. Comparison of top tension statistics of both cases show that the extreme top tension of production riser of Case A Spar is slightly increased, but the standard deviation is increased significantly. The large standard deviation in axial tension may causes increased fatigue of riser system. The most loaded mooring line (i.e. M2 mooring in Fig. 5) top tension is shown in Fig. 30 through 32. Fig. 32 shows that Case A and Case B Spar have almost identical mooring top tension except for a small peak in heave natural period zone for Case A Spar. This means that the heave motion effect on the most loaded line is not significant. A summary of the most loaded line statistic is shown in Table 9.

Table 6 100-year hurricane condition statistics (CASE A)

	Surge	Sway	Heave	Roll	Pitch	Yaw
	(m)	(m)	(m)	(deg)	(deg)	(deg)
MEAN	2.23E+1	-4.71E+0	-3.43E-1	4.47E-1	-1.63E+0	-1.77E+0
STD	2.01E+0	1.16E+0	2.52E-1	3.49E-1	9.00E-1	2.60E-1
EXE	-2.84E+1	7.79E+0	-1.31E+0	1.49E+0	-5.48E+0	-2.85E+0
LF	1.91E+0		7.07E-02		6.24E-1	
WF	6.31E-1		2.42E-01		6.44E-1	

Note) STD: standard deviation, EXE: extreme, LF: low frequency, WF: wave frequency

Table 7 100-year hurricane condition statistics (CASE B)

	Surge	Sway	Heave	Roll	Pitch	Yaw
	(m)	(m)	(m)	(deg)	(deg)	(deg)
MEAN	2.22E+1	-4.71E+0	-2.39E-1	3.80E-1	-1.64E+0	-2.26E+0
STD	2.02E+0	1.17E+0	1.02E-1	3.52E-1	9.04E-1	6.48E-1
EXE	-2.84E+1	7.80E+0	-7.09E-1	1.51E+0	-5.52E+0	4.18E+0
LF	1.91E+0		7.18E-2		6.32E-1	
WF	6.31E-1		6.96E-1		6.42E-1	

Note) STD: standard deviation, EXE: extreme, LF: low frequency, WF: wave frequency

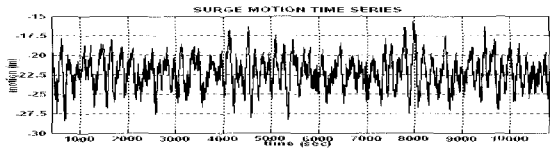

Fig. 17 Surge response time series (CASE A)

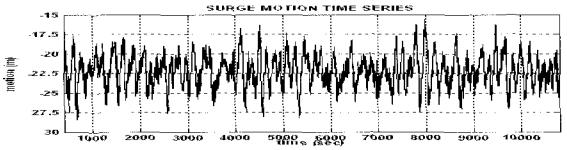

Fig. 18 Surge response time series (CASE B)

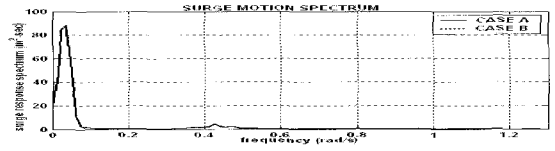

Fig. 19 Surge response spectrum (CASE A and CASE B)

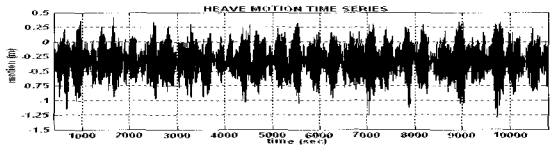

Fig. 20 Heave response time series (CASE A)

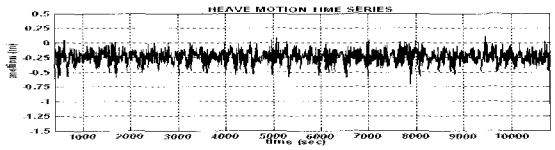

Fig. 21 Heave response time series (CASE B)

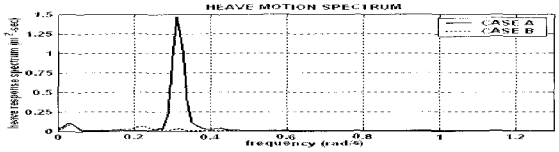

Fig. 22 Heave response spectrum (CASE A and CASE B)

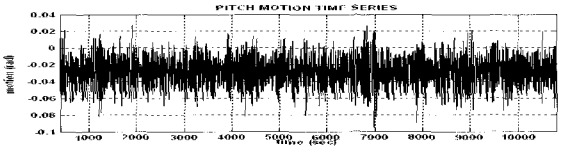

Fig. 23 Pitch response time series (CASE A)

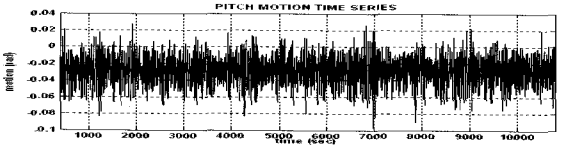

Fig. 24 Pitch response time series (CASE B)

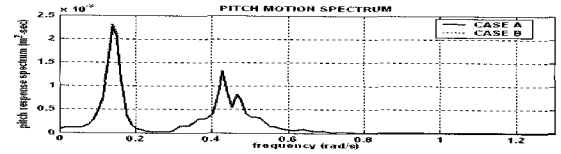

Fig. 25 Pitch response spectrum

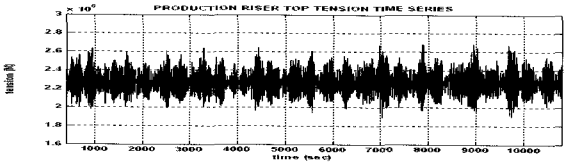

Fig. 26 Production riser top tension time series (CASE A)

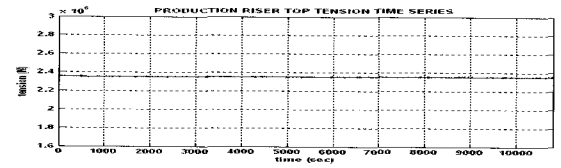

Fig. 27 Production riser top tension time series (CASE B)

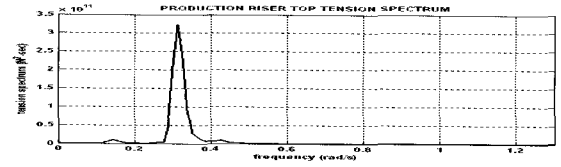

Fig. 28 Production riser top tension spectrum (CASE A)

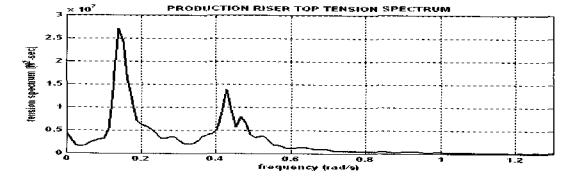

Fig. 29 Production riser top tension spectrum (CASE B)

Table 8 Production riser top tension statistics

	MEAN	STD	EXE	LF	WF
	(N)	(N)	(N)	(N)	(N)
CASE A	2.27E+6	1.17E+5	2.68E+6	2.34E+4	1.14E+5
CASE B	2.35E+6	1.94E+3	2.38E+6	1.24E+3	1.41E+3

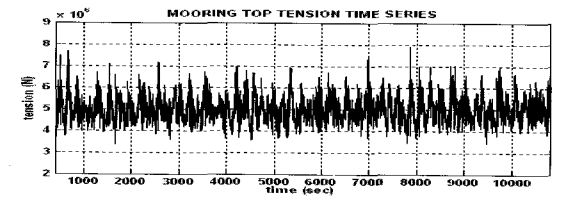

Fig. 30 Most loaded line top tension time series (CASE A)

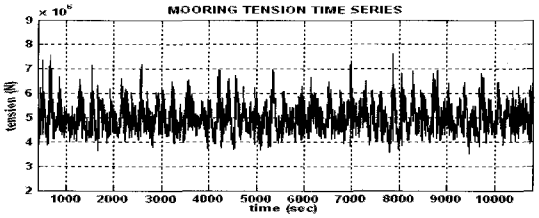

Fig. 31 Most loaded line top tension time series (CASE B)

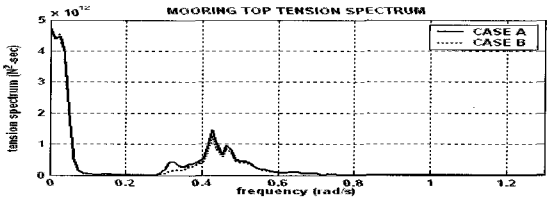

Fig. 32 Most loaded line top tension spectrum

Table 9 Most loaded line top tension statistics

	MEAN	STD	EXE	LF	WF
	(N)	(N)	(N)	(N)	(N)
CASE A	4.96E+6	6.25E+5	7.90E+6	4.77E+4	4.03E+5
CASE B	4.96E+6	6.03E+5	7.62E+6	4.79E+3	3.67E+3

6. CONCLUSION

The pneumatic riser support system is compared with the buoyancy-can riser support system by newly developed numerical scheme for modeling the effects of the riser support system inside of spar moon-pool in the free decay test as well as the 100-year hurricane conditions of Gulf of Mexico. The free decay simulation results show that pneumatic cylinders change the heave motion significantly because there is additional heave restoring force from pneumatic cylinders. The 100-year hurricane simulation results show that the pneumatic riser support system produces larger heave motion. The reason is that the pneumatic riser support system decreases the spar natural period in heave direction, and thus the spar platform more exposed to wave energy. The pneumatic riser support system increases the riser top tension compared with the buoyancy-can riser support system. Because risers are hanging off the spar platform with the pneumatic cylinder, the pneumatic riser support system also increases the spar platform payload. Thus, the buoyancy-can riser support system produces smaller spar hull motions, and there is less top tension in the vertical riser system. In Holstein spar, the risers are supported by pneumatic cylinders. However, Due to large heave motion, Holstein spar uses additional damping system to reduce heave motion.

REFERENCES

ANSI/API RP-2A WSD (1994). Recommended Practice for Planning, Designing and Constructing Fixed Offshore Platforms Working Stress Design, American Petroleum Institute, pp 23.

Garrett, D.L. (1982). "Dynamic Analysis of Slender Rrods", Journal Energy Resources Technology, Vol 104, pp 302-307.

Gupta, H., Finn, L.D., and Weaver, T.O. (2000). "Effects of Spar Coupled Analysis", Offshore Technology Conference, (OTC 12082), Houston, Texas.

Kim, C.H., Kim, M.H., Liu, Y.H., and Zhao, C.T. (1994). "Time Domain Simulation of Nonlinear Response of a Coupled TLP System", International Journal of Offshore and Polar Engineering, Vol 4, No 4, pp 281-291.

Kim, M.H., Roesset, J.M., and Zhang, J. (1997). "Nonlinear Dynamic Analysis Methods for Spar Platforms", Proceedings of the Society of Naval Architect and Marin Engineer Conference (Gulf Section), Huoston, Texas.

Kim, M.H., Tahar, A., and Kim, Y.B. (2001). "Variability of Spar Motion Analysis against Various Design Methodologies/Pparameters", Proceedings of the 20th Offshore Mechanics and Artic Engineering, OMAE 01-OFT1063 [CD-ROM].

Koo, B. J. (2003). "Evaluation of the Effect of Contact between Risers and Guide Frames on Offshore Spar Platform", Ph.D. Dissertation, Civil Engineering Department, Texas A&M University, College Station, TX.

Koo, B.J., Kim, M.H., and Randall, R.E. (2004a). "Mathieu Instability of a Spar Platform with Mooring and Risers", Journal of Ocean Engineering, Vol 31, pp 2175-2208.

Koo, B.J., Kim, M.H., and Randall, R.E. (2004b). "The Effect of Nonlinear Multi-contact Coupling with Gap between Risers and Guide Frames on Global Spar Motion Analysis", Journal of Ocean Engineering, Vol 31, pp 1469-1502.

Lee, C.H., (1995), WAMIT Theory Manual, Department of Ocean Engineering, MIT, MA.

Ma, W., Lee, M.Y., Zou, J., and Huang, E.W. (2000). "Deepwater Nonlinear Coupled Analysis Tool", Offshore Technology Conference, (OTC 12085), Houston, TX.

Paulling, J.R., and Webster, W.C. (1986). "A Consistent Large-amplitude Analysis of the Coupled Response of a TLP and Tendon System", Proceeding of the 5th Offshore Mechanics and Arctic Engineering Symposium, Vol 3, pp 126-133.

Ran, Z., and Kim, M.H. (1997). "Nonlinear Coupled Responses of a Tethered Spar Platform in Waves", International Journal of Offshore and Polar Engineering, Vol 7, No 2, pp 111-118.

Ran, Z., Kim, M.H. and Zheng, W. (1999). "Coupled Dynamic Analysis of a Moored Spar in Random Waves and Current (Time-Domain Vs. Frequency-Domain Analysis)", Journal of Offshore Mechanics and Artic Engineering, Vol 121, pp 194-199.

Tahar, A., Ran, Z., Kim, M.H., (2002). "Hull/Mooring/Riser Coupled Spar Motion Analysis with Buoyancy-can Effect", Proceedings of the 12th International Offshore and Polar Engineering Conference, pp 223-230.

2005년 6월 16일 원고 접수
2005년 10월 13일 최종 수정본 채택